OSI SAF
Visiting Scientist Activity Report
AVS_2017_05

Final Report

Inter-comparison of high and low microwave frequency sea ice concentration algorithms

Version 1

Prepared by Carolina Gabarró and Mukesh Gupta
Revised by Rasmus T. Tonboe and Thomas Lavergne

October 2018

Proposal Summary

VSA title	***Intercomparison of high and low microwave frequency sea ice concentration algorithms***		
VSA proposal ID:	AVS_201705	***Objective category:***	"Intercomparison"
VSA Host institute:		***Related SAF products:***	OSI-401, OSI-408, OSI-450
VSA supervisor:	Rasmus Tonboe Thomas Lavergne	***Related SAF WP:***	WP 2XXXX
Expected start date:	01-10-2017	***Related SAF (review) processes:***	
Expected end date:	24-10-2018	***VSA costs:***	10407 €
VS candidate:	Carolina Gabarro	***VS / AS:***	AS
Document prepared by	Carolina Gabarro and Mukesh Gupta		

Content

1.- Objective

The objective of this associated scientist project is to inter-compare the sea ice concentration from microwave radiometers, for winter and autumn period, at low microwave frequency to current OSI SAF sea ice concentration products, in particular: the OSI-401 based on SSMIS data and the OSI-408 based on AMSR data along the lines of the sea ice concentration intercomparison described by Ivanova et al. (2015). New algorithms recently developed in the ESA CCI project (Clime Change Initiative) and published in the OSI-450 CDR will be included as well. Therefore, the activity is also of interest to the OSI-409/OSI-409-a and the OSI-430 and OSI-450 which are climate data records (CDR).

It has been demonstrated that sea ice concentrations derived from low frequency microwave radiometer data has a low noise level, during summer, over open water from the atmosphere and over ice due to low ice surface emissivity variability (Ivanova et al. 2015, Gabarro et al. 2017). This is also true during summer melt. However, low frequency channels have coarse spatial resolution and at L-band there is an ambiguity between sea ice concentration and the thickness of thin ice. Further the continuity of L - and C - band radiometers in space is uncertain.

The ESA sea ice concentration round robin data package (RRDP) will be used as an independent reference in the intercomparison and for analysing the algorithms at fixed tie-points. Recommendations are given on the evaluation methodology itself as a contribution to the

discussion on the development of the OSI SAF monitoring and validation procedure.

The main difference with respect to the work done in the previous AVS - 16-03 is that the previous one was specifically focused on summer period, and had the objective to improve the selected region used by OSISAF method to determine the 100% ice tie points.

The objective of this proposal is to investigate and compare the low frequency algorithms with the current sea ice concentration algorithms and the algorithms developed in the ESA CCI project and which may be future OSISAF algorithms.

Tasks and methods

- Set up software to inter-compare the different sea ice concentration products for a selected period (autumn and winter period).
- As a reference and independent measure each of the products will be compared to the ESA round robin data package (RRDP).
- Collocate the different products and compute statistics.
- Comparison of SIC computed with new algorithms using 6 GHz radiometer band proposed by L. Toudal (personal communication) and Thomas Lavergne.
- Compare results with the SMOS SIC algorithm proposed in Gabarro et al 2017.

The Scientific analysis has been divided in different parts: First a comparison of the different algorithms just in regions of high SIC is exposed. Then an analysis of the random error of the different algorithms is presented. An analysis of the systematic errors is performed to determine the spatial biases observed during winter. Finally, a sensitivity analysis of the different SIC algorithm to the temperature in the snow-ice interface, the snow depth, ice thickness and air temperature is presented.

2.- Data Set Used

The RRDB data base is used. The files from the RRDP SICCI-RRDP-V1_1 have been used for year 2007-2011, and 2013- 2015. Take into account that 2007-2011 uses AMSR-E while the rest uses AMSR-2. This data file contains collocated AMSR data with other satellites data, models and in situ measurements. The files used are:

1.- The data from the file called SICCI-RRDP-ASCAT-vs-AMSR-vs-ERA-vs-DTUSIC1-200X-N.text has been used. It contains TB from AMSR (all bands) collocated with high sea ice concentration pixels identified by DTU analysis from SAR data. ASCAT and ERA atmospheric data are also collocated. Used in section 4.

2.- The data from the file called SICCI-RRDP-ASCAT-vs-AMSR2-vs-ERA-vs-IMBCRREL20XX.text has been used. It contains TB from AMSR (all bands) collocated with temperature profile data from IMBB profilers. ASCAT and ERA atmospheric data are also collocated. Used in section 6.

3.- AMSR-2 data from November 2013 to March 2014. This data is in EASE2 grid of 25 km but has been resampled to 50km to have the same grid than the SICCI dataset. SICCI2 SIC dataset is also used which has a 50km resolutions. These SICCI2 products are downloaded from data.ceda.ac.uk webpage. These data is used at section 5.

4. Operational Ice Bridge data collocated with AMSR2 data from 2014 from the RRDB dataset. The OIB files called SICCI-RRDP-ASCAT-vs-AMSR2-vs-ERA-vs-NERSC-OIB-201403XX.text from the 13,21,26,28 and 31 March 2014 are used in section 7.

3.- Sea Ice Concentration algorithms presentation

The SIC models used for the analysis are summarized below (and also in the Final Report of the previous OSI_AVS_16_03). The electromagnetic frequency of the different channels used by the algorithms are specified. Further, we also classify the algorithms into polarization type, frequency type or mixed according to their algorithm to do a sensitivity analysis of the different type of algorithms to various type of noise and biases. The algorithms analysed are the following:

a) **NASA Team** (Markus and Cavalieri 2000, uses 19H, 19V, 37V) → Polarization
b) **Bristol** (Smith 1996 uses 19V, 37V, 37H) → frequency
c) **Bootstrap F** (Comiso 1986; uses 19V 37 GHz V, 37H) → frequency
d) **Bootstrap P** (Comiso 1986; uses 37 H, 37V) → polarization
e) **Two channel** at 10 GHz (uses 10H, 10 V) → polarization

SIC=1.33313-0.01686*(TB10H-TB10V)

f) **One Channel** algorithm (Pedersen (1994), uses 6.9 GHz H), which computes the SIC as:

SIC = (TB6.9H – OW_TP)/(Ice_TP – OW_TP)

The models One_adap.H and One_adap.V are adaptation of model f), with new Tie Points values and using V-pol. → One polarization

g) **LTP637:** algorithm proposed by Leif Toudal uses TB6V, TB37V, wind speed and skin temperature from NWP/ERA. → frequency

h) **SICCI2-50km:** provided by T. Lavergne et al 2018 uses 6V and 37H and 37V. It takes into account SIC values larger than 100%. This is the unique algorithm that uses dynamic tie points. Data have been downloaded from data.ceda.ac.uk webpage and have been collocated with SAR data (nearest). → mixed

i) **LowFreq algorithm:** provided by T. Lavergne, uses 6GHZ V-pol, 10 GHZ V-pol and 18GHz V-pol from AMSR. The TP are tuned for AMSRE. → frequency

j**) SMOS algorithm:** described by Gabarro et al 2017. It uses the angular difference of TB V-pol at 1.4GHz. The highest limit is 110% → One polarization

g) **SIC models using emissivity** (and not Tbs) proposed in the previous VS report (Gabarro et al. 2016) has also been tested. Emissivity is computed as TB6.9/SkinTemp (SkinTemp obtained from

NWP). → One Polarization

SIC(Emis) = (EMIS 6.9V/H – OW_TP)/(Ice_TP – OW_TP)

All the algorithms were evaluated without applying open water/weather filters, since our aim was a comparison of the algorithm sensitivities. The tie points are static (constant in time) and are specified in Annex 2, except the SICCI2 algorithm that used dynamic tie points.

Table 1 below summarize the methodology and bands used for the different analyzed SIC algorithms.

Algorithm	Freq used	Type Ratio	Low frequency bands
NasaTeam	19V,19H,37V	Polarization	NO
BRISTOL	19V, 37H, 37V	Frequency	NO
BOOTSTRAP_F	19V, 37V, 37H	Frequency	NO
BOOTSTRAP_P	37H, 37 V	Polarization	NO
Two Channel	10H, 10V	Polarization	YES
OneChannel	10H	One pol	YES
LTP637 - Tphys	6V, 37V	Frequency + atmospheric	YES
SICCI2-50km	6V, 37V, 37H	Mixed	YES
LowFreq	6V, 10V, 19V	Frequency	YES
SMOS	1.4V	One pol.	YES
Emis6.9V	6.9 V	One pol.+atm	YES
Emis6.9 H	6.9 H	One pol.+atm	YES

Table 1: Resume of the algorithms used in the analysis specifying methodology and if low frequency bands are used or not. We consider low frequency bands those lower or equal to 10 GHz.

4.- SIC algorithm performance comparison

In this section we inter-compare the different SIC algorithms used in the study. The analysis is done with AMSR-2 (tc_amsr2_nh_ease2-250_YYYYMMDD12000.nc) TB from November 2013 to March

2014 (winter period). The TB maps are at 25km resolution, but those have been extrapolated to 50 Km resolution to have the same resolution as the SICCI2 maps. An averaged SIC winter product is computed by time averaging SIC, per grid point, considering only pixels with SIC values larger than 80%. So the equation results as:

$$\overline{SIC}(x,y) = \sum_{t} SIC(x,y,t)$$

Figure 1 shows the scatterplots between algorithms as well as the correlation factor. Histograms of each of the algorithms are plotted in Annex 1.

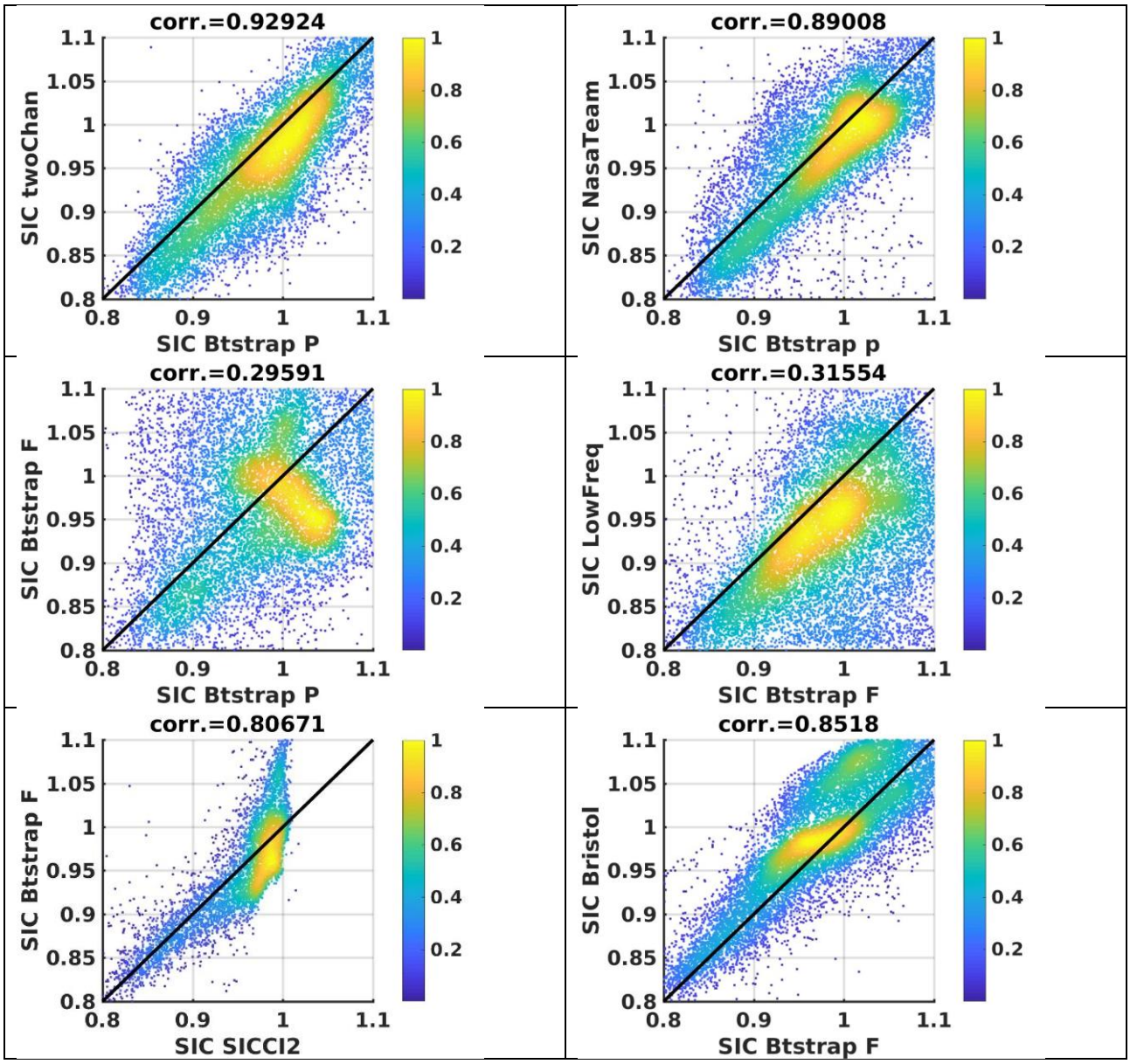

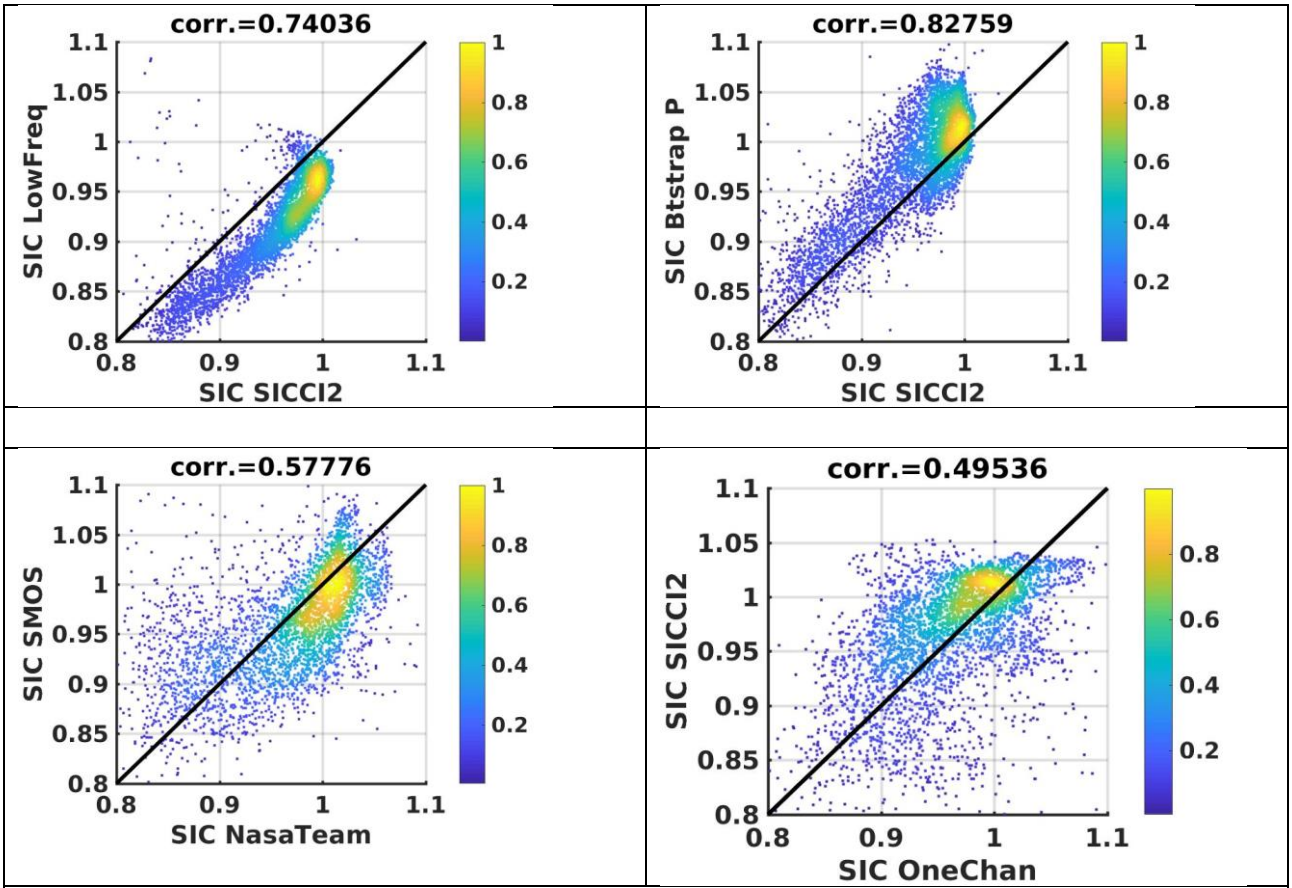

Figure 1: Scatter plot with the correlation factor of different SIC algorithms

From Figure 1 one can observe that when comparing algorithms which uses same methodology (FR or PR) the scatter plots show a narrow line and correlation is high, while the scatterplots of different methodological algorithms show a larger dispersion and the correlation values reduces. For example, the scatter plot between Bootstrap F (FR) vs Bootstrap P (PR), show large dispersion and low correlation. While when comparing same methodology algorithms, correlation increases and the dispersion is reduced (i.e. Bootstrap-F vs SICCI2, Bristol vs Bootstrap F, Bootstrap-P vs Two Channel)). The SICCI2 algorithm show a high limit value near 1, which is also observed with the histograms shown in annex 1.

	NT	Bristol	BtsF	Bts P	2Chan	1Chan	SICCI2	LowFrq	SMOS
NT		0.87	0.53	0.89	0.92	0.86	0.74	0.57	0.58
Bristol			0.85	0.71	0.71	0.86	0.92	0.57	0.49
Bts-F				0.29	0.31	0.55	0.81	0.32	0.93
Bts-P					0.92	0.86	0.83	0.61	0.47
2Chan						0.86	0.66	0.58	0.45
1Chan							0.92	0.77	0.50
SICCI2								0.74	0.50
LowFrq									0.57
SMOS									

Table 2: Correlations factor between algorithms. Color codes: Frequency type (red), polarization type (green), Mixed (Blue), none of the previous (white).

Table 2 shows the correlations value between algorithms. The correlations are higher for those algorithm which uses same methodology (FR/PR, or one and mixed). On the other hand, Low Frequency bands and SMOS algorithms show low correlation with respect the rest to the models.

5.- Study on random errors for 100% ice pixels:

In this section we study the random errors of the SIC product for closed ice pixels for each of the proposed models. These pixels with large SIC determined by SAR dataset processed by DTU have been collocated with AMSR data. Then the SIC is computed by using the proposed algorithms with the AMSRE/2 data.

The closed ice pixels are classified in areas of high sea-ice concentration and after 24h of convergent sea ice motion, as computed from a highly accurate SAR-based sea-ice drift product from the Copernicus Marine Environment Monitoring Service (CMEMS, http://marine.copernicus.eu). This RRDP files are described in more details in Ivanova et al. (2015).

In fact, in this section we do a validation against a ground truth which is the SAR determined SIC.

These files also contain atmospheric information, which is required for the LTP637 algorithm (need skin temperature and wind speed information) and the emissivity algorithms (need Skin temperature).

Table 3 resumes the STD and mean values for closed ice between November and April only (fall and winter period) during several years. One can observe that all the algorithms produce SIC>100%, result which is expected since the TB values can have larger values than the Tie Points. In fact, this is required to compute the STD and mean properly and to avoid biases. Latter one, the SIC values larger than 100 are set to 100%.

Table 4 resumes the STD and mean values globally for all the years and **classifies the algorithms** between two categories: 1) uses frequency ratio/polarization ratio/mixed/others and 2) uses low frequency bands (1.4, 6.9 and 10 GHz)/Not using low frequency bands. The algorithm which present more stable results (less STD) have been emphasized in yellow and are the following: LTP637 model, SICCI2-50km model, LowFreq and the Emissivity model at 6.9Ghz, specially using the V-pol. One can observe that all cases uses low frequency bands. Figure 2 shows the same values in a graphic.

SICCI2-50km (in addition to using low frequencies) implements a number of optimizations that the other algorithms (including the new "LowFreq") lack (more info of the algorithm can be found in Lavergne et al 2018), as for example this method uses dynamic TP. The values from the SICCI2-50km dataset used in this analysis, are not limited to 100% (as the SIC product is). When SIC=100% we use the raw data (which has values larger than 100%), to avoid biased results.

To compute the Emis6.9V SIC product we use the collocated skin temperature from the NWP field (in this case from the ERA-Interim). So we compute the emissivity by doing: TB/Tskin. They both have the same spatial resolution. The tie points values are also computed from the emissivity values.

	2007	2008	2009	2010	2011	2013	2014	2015
	Mean;std	Mean;std	Mean;std	Mean;std	Mean;std	Mean;std	Mean;std	Mean;std
Nasa	105.08;6.73	98.45;5.04	100.38;4.35	98.34;2.83	99;3.78	94.91;6.11	96.9;6.76	99.52;3.45
Bristol	103.98;3.9	99.45;4.35	99.25;3.61	100.53;3.07	101.18;3.16	98.81;2.21	100.2;2.75	99.43;3.46
Bootstrap F	102.61;7.74	98.64;6.38	98.32;6.73	102.28;5.15	103.28;4.1	100.42;2.67	102.7;3.41	99.12;6.06
Bootstrap P	106.34;8.96	100.83;4.62	100.83;4.87	97.54;3.45	97.58;5.25	95.96;6.82	95.8;8.24	99.98;4.1
TwoChan 10G	102.21;8.19	96.52;6.37	99.75;6.34	96.62;4.22	97.61;4.71	92.2;7.08	95.08;8.02	98.57;5.11
One Chan	102.28;2.53	98.16;4.35	99.4;2.71	99;2.39	101.38;2.74	100.64;4.09	101.88;4.46	100.08;4.01
One Chan Adapt H	92.81;2.22	89.2;3.81	90.28;2.38	89.94;2.09	92.02;2.4	92.12;3.62	93.22;3.95	91.63;3.54
One Chan Adapt V	89.17;2.15	87.17;4.14	87.49;3	88.47;2.24	91.48;2.55	92.8;3.18	92.8;3.47	89.35;3.88
LTP37	99.52;3.24	97.47;2.9	97.73;2.61	98.22;2	98.59;1.71	99.78;1.59	100.95;2.15	98.06;2.95
SICCI2-50	98.74;2.31	99.24;1.72	99.04;2.2	99.5;1.52	99.68;1.55	99.27;2.01	99.7;2.3	99.89;2.09
LowFreq	102.26;2.68	99.76;2.76	99.92;1.99	99.22;1.99	100.65;1.9	97.44;2.11	96.23;3.65	94.42;2.77
SMOS	-	-	-	-	-	96.98;6.1	93.73;8.05	93.6;4.9
Emis 6.9 H	92.68; 1.52	90.36;2.21	91.01;1.58	90.3;1.89	89.35;1.49	89.78:2.3	90.96:2.76	91.18;1.79
Emis 6.9 V	100.5;2.43	99.37;1.57	99.78;1.83	99.66;1.82	98.35:1.21	99.3;1.57	99.8;1.79	99.78;1.51

Table 3: Mean and STD SIC values for several algorithms with AMSR data only for those pixels which are considered SIC=100 % by the SAR data, from November to April. Take into account that 2007-2011 uses AMSR-E while the rest uses AMSR-2.

	Ratio/Low freq	Mean	STD
Nasa team	Mixed /NO	99.07	4.88
Bristol	FR /NO	100.35	3.31
Bootstrap F	FR/NO	100.82	5.28
Bootstrap P	PR/NO	99.38	5.79
TwoChan 10G	PR / YES	97.32	6.26
One Chan	Other/ YES	100.35	3.41
One Chan Adapt H	Other/ YES	91.4	3.00
One Chan Adapt V	Other/ YES	89.84	3.08
LTP37	FR/YES	98.79	2.39
SICCI2-50	Mixed/YES	99.38	1.95
LowFreq	FR/YES	98.74	2.48
SMOS	Other/YES	95.77	6.35
Emis 6.9 H	Other/YES	90.70	1.94
Emis 6.9 V	Other/YES	99.61	1.75

Table 4: Mean and STD SIC values for several algorithms with AMSR data only for those pixels classified as close ice by the SAR data, from November to April for all the years. Yellow columns indicate that the STD is lower or equal 3.

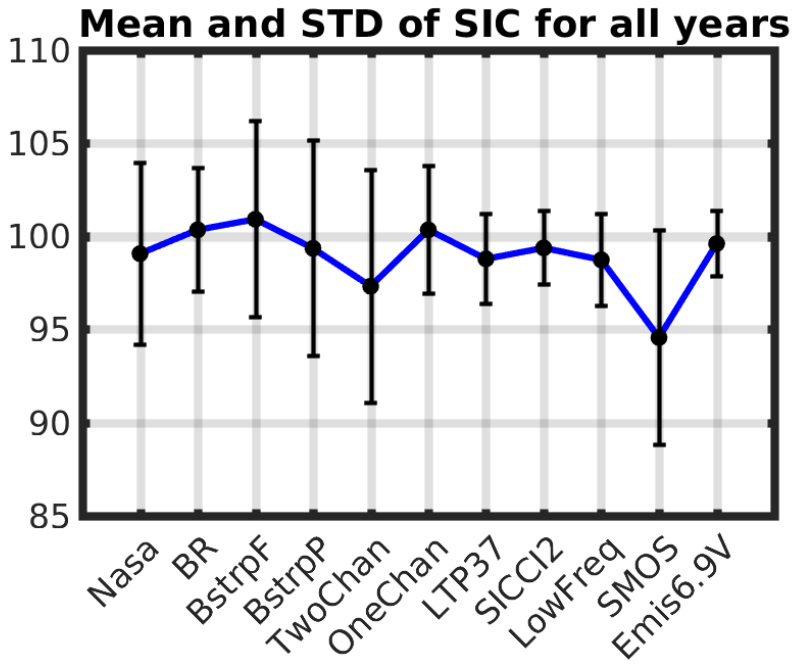

Figure 2: Same information as table 3. Mean and STD SIC values for several algorithms with AMSR data only for those pixels classified with SIC=100% by the SAR data, from November to April for all the years.

Results from Table 4 are comparable with results from table 2 of Ivanova et al. 2015. In that paper, they similarly compute the STD of the SIC obtained with different models only for high Sea Ice Concentration pixels. Those measurements are not only limited to winter. However, only few models from that analysis match with the models studied here. The models used in both analyses are: Brictol, NasaTeam, OneChannel and Bootsratp-P. The differences observed are of around 10% on the STD.

Conclusions: LTP637, SICCI2-50km, LowFreq and the Emis6.9V are the models with better stability (less STD) during winter for regions with high concentration of sea ice**. The one channel Adapt also show low STD but have a clear problem with the Tie-points used. Moreover, those algorithms present very near 100% mean value. An important observation is that the models with lowest STD use the low frequency bands (uses 1.4, 6 or 10GHz), which present more precise Tb values as already stated in the conclusions of the AVS- 16-03.**

6.- Spatial and temporal biases analysis

In this section, we analyze the systematic error (biases) of different SIC algorithms for pixels with high sea ice concentration. AMSR-2 TB maps at different bands have been used.

The systematic error is estimated by computing the SIC averaged in time (only winter period), per grid point, considering only pixels with SIC values larger than 80%, as described in section 4. Then, the spatial bias is estimated by subtracting 1 from the mean SIC (since we expect to have 100% sea ice concentration). So the equation results as:

$$\overline{SIC}(x,y) = \sum_{t} SIC(x,y,t)$$

$$\Delta SIC(x,y) = (\overline{SIC}(x,y) - 1)$$

The temporal variability is also computed as the Standard deviation on time of the maps $\sigma\big(SIC(x,y)\big) = STD\big(SIC(x,y,t)\big)$.

The systematic error maps (bias) and the temporal variability (STD in the time domain), for the different algorithms are shown in figure 3. Value of STD in the bottom of the figure indicates the spatial STD of the bias maps. Figure 3b is the bias map normalized to the product-specific variability.

SIC using algorithms LTP37 and EmisV/H are not compute since they need skin temperature of the ice, and we don't have this variable collocated with this AMRS2 TBs.

Systematic bias observed in close ice regions might be due to surface emissivity variability (due to ice type, temperature of the emission layer, snow depth, etc…) over closed ice.

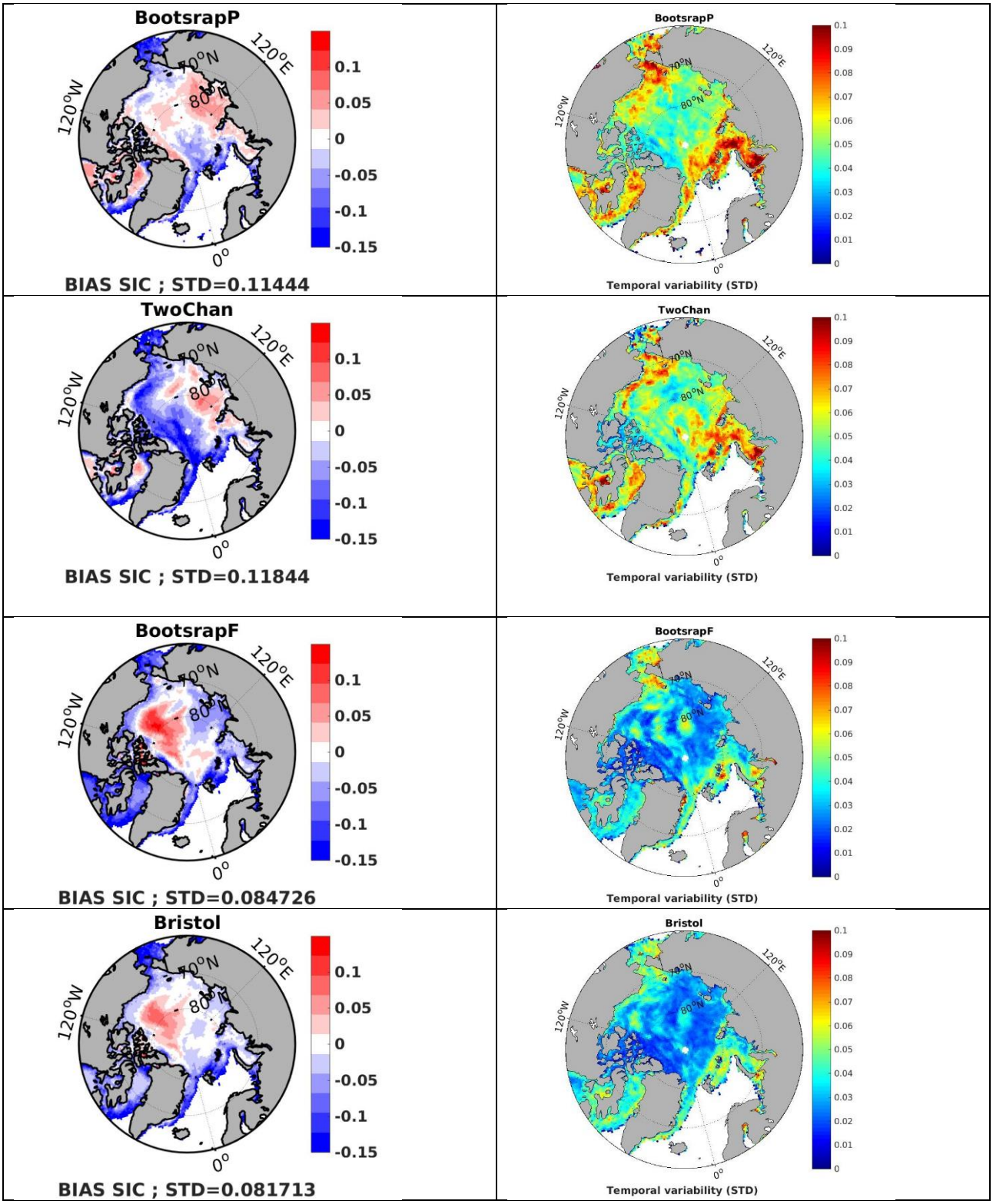
BootsrapP
120°W
120°E
70°N
80°N
0°
0.1
0.05
0
-0.05
-0.1
-0.15
BIAS SIC ; STD=0.11444
BootsrapP
0.1
0.09
0.08
0.07
0.06
0.05
0.04
0.03
0.02
0.01
0
Temporal variability (STD)
TwoChan
BIAS SIC ; STD=0.11844
TwoChan
Temporal variability (STD)
BootsrapF
BIAS SIC ; STD=0.084726
BootsrapF
Temporal variability (STD)
Bristol
BIAS SIC ; STD=0.081713
Bristol
Temporal variability (STD)

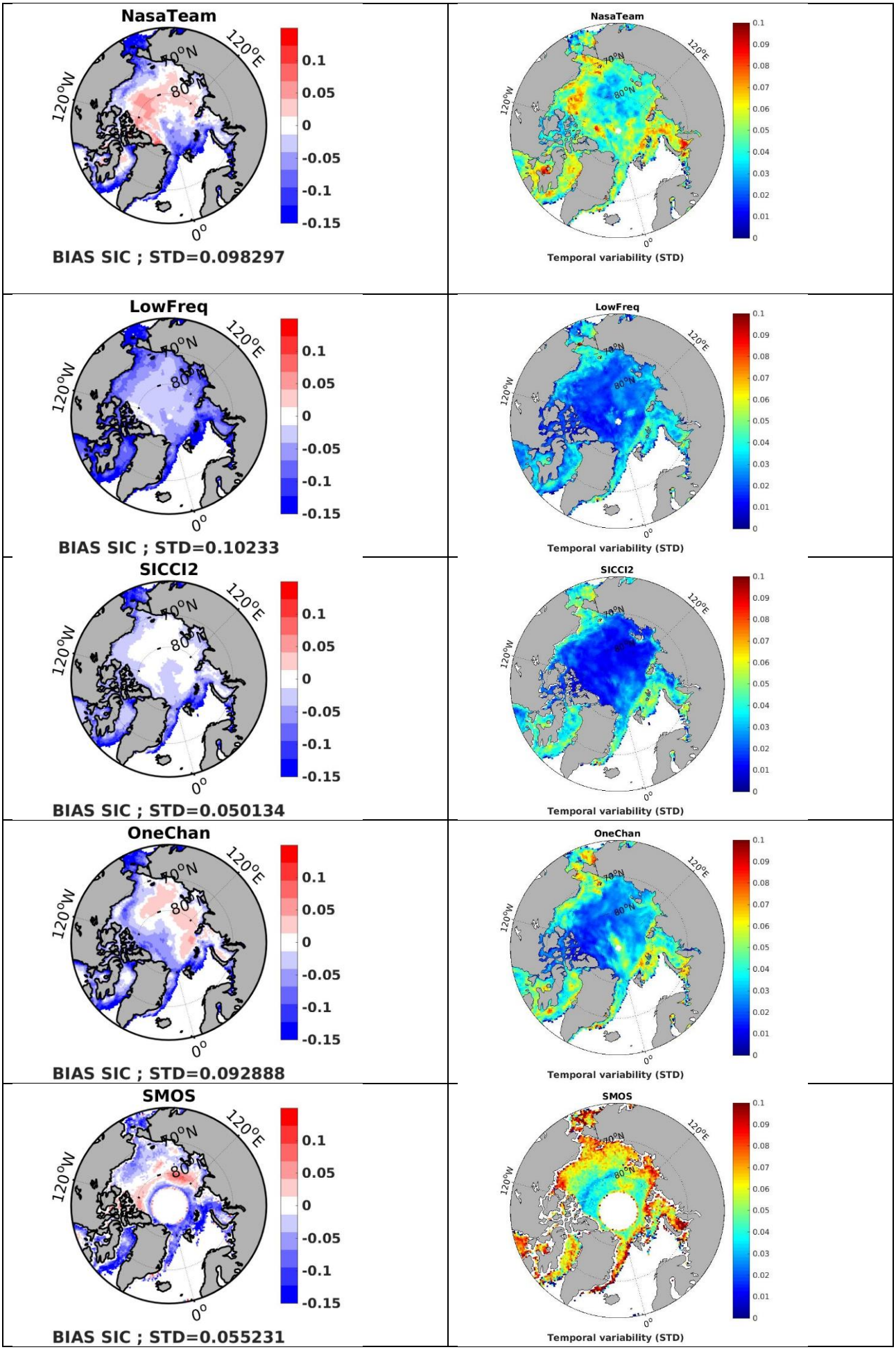
NasaTeam
120°W
120°E
70°N
80°N
0°
0.1
0.05
0
-0.05
-0.1
-0.15
BIAS SIC ; STD=0.098297
NasaTeam
0.1
0.09
0.08
0.07
0.06
0.05
0.04
0.03
0.02
0.01
0
Temporal variability (STD)
LowFreq
BIAS SIC ; STD=0.10233
LowFreq
Temporal variability (STD)
SICCI2
BIAS SIC ; STD=0.050134
SICCI2
Temporal variability (STD)
OneChan
BIAS SIC ; STD=0.092888
OneChan
Temporal variability (STD)
SMOS
BIAS SIC ; STD=0.055231
SMOS
Temporal variability (STD)

Figure 3: Left: Systematic error of high concentration SIC, the legend shows the STD of the spatial bias. Right: Temporal variability per pixel.

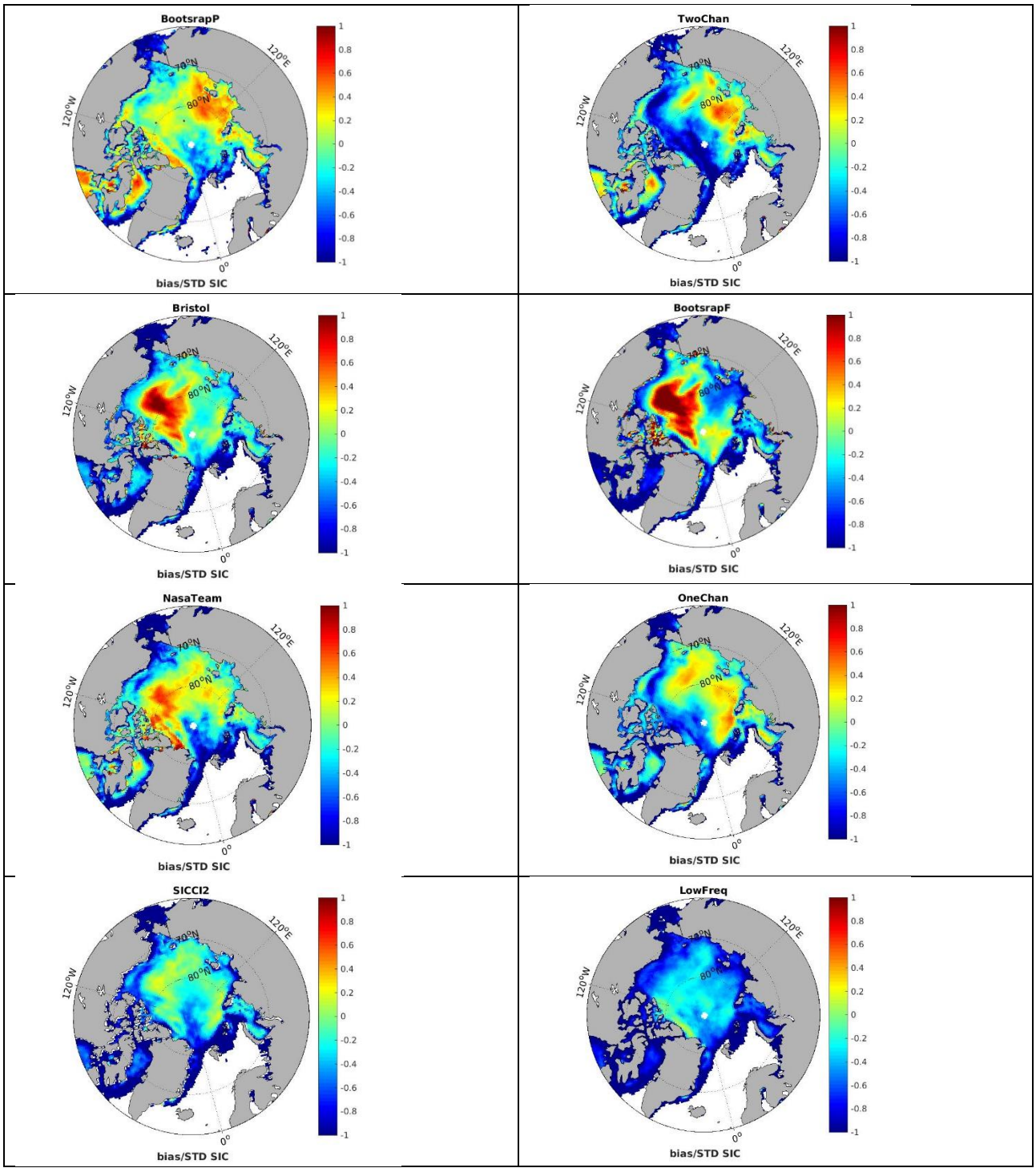

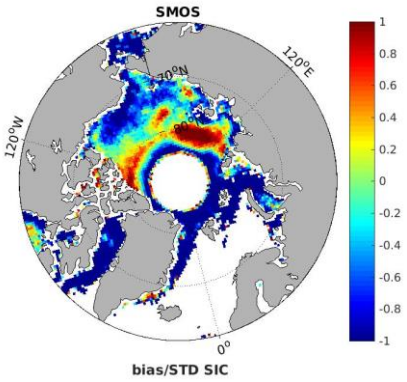

Figure 3b: Systematic error of high sea ice concentration SIC divided by the systematic STD**.**

The Polarization type algorithms (BootstrapP and Two Channel), have similar bias pattern as well as the temporal std, indicating positive bias in the Russian region, and larger temporal variability near the MIZ zones, which is expected.

BootstrapF, Bristol agorithms (FR algorithms & high frequency bands) and NasaTeam (polarization type & high frequency bands) show also similar pattern between them: large regional differences and an important positive bias in the multi-year ice region (north of Canada) which is also reported in Lavergne et al 2018. This bias in multi-year ice is also observed in SICCI2 data but is corrected with different techniques. On the contrary, the temporal std is lower than that for the PR algorithms.

Moreover, those maps show a feature near Ellesmere Island, and Canadian coast with large contrast in relatively small distance, while the ice type has not been changed. We will analyze the cause of this issue with Operation Ice Bridge (OIB) data (see section 7).

The algorithms using low frequency bands show much lower bias and also very low temporal STD, except the SMOS map. SMOS suffers from biases in latitude 80º, probably due to the acquisition form (lower accuracy in the edges of the track) and also due to using only one band and one polarization. The largest variability is in the MIZ zone, which is expected since the SMOS SIC quality is limited when thin ice is present.

The spatial variability, STD of the bias are between 5% and 12% in all the algorithms.

The SICCI2 STD is very low (right figure) and this is also evidenced in the histograms from Annex 1. We expect that the algorithms which uses static tie points, present larger temporal variability, than the one with dynamic tie-points (SICCI2 only). Another reason for the good accuracy of the SICCI2 algorithm is that this method uses novel correction scheme (Lavergne et al., 2018) that effectively mitigates most of the systematic errors over the basin. The method, prior to the corrections, in was underestimating the SIC especially on the Central basin and was overestimating the SIC of the first year ice. The use a curvy ice line is one of the corrections applied, which adjust those systematic errors (Lavergne et al., 2018).

Conclusion on Systematic error analysis:

- Among all, the **LowFreq** (6V, 10V, and 18V GHz) and **SICCI2** (6V and 37H, V) SIC maps show less systematic error and also less temporal variability in high SIC regions. The low bias might be due to the use of low frequency bands and probably for the fact that they use 3 bands. Greater the number of frequencies more information available from the target (i.e. sea ice). This is in agreement with the results from previous OSISAF work (Gabarro et al, 2017) where they observed that the low frequency TB bands have less systematic and random errors. The lower temporal variability of SICCI2-50km might be due to the fact that this algorithm uses dynamic type-points.

- Algorithms based on the polarization only (**Bootstrap P, TwoChan**) show higher systematic error in the coast, ice edge, and thin ice regions (Russian coast). TwoChan seems to delineate information on the ice type characterization at 10 GHz.

- Algorithms based on the 19/37GHz **frequency** (**Bootstrap F, Bristol**) show high positive bias in the thick ice regions in the Canada Basin. Possible reason for that might be the deformation of the ice surface roughness (scattering) or snow cover. The gradient ratio between the channels 10 and 37GHz V-pol is used to retrieve the snow depth (Markus and Cavalieri, 1998). In fact, snow cover and depth reduce TBV specially at 10, 19 and 37Ghz and therefore reduce the SIC (Kilic, 2017). Region north of Ellesmere Island is the region with largest snow cover (see figure bellow) therefore the negative bias could be due to the high snow depth. This will be analyzed in the section 7.

- OneChan algorithm shows negative systematic error on the ice edge region. Maybe due to the use of low frequency band (6Ghz) which has certain penetration, and problems when thin ice is present.

- SMOS also presents a lot of variability in the thin ice region, where it produces an underestimation of SIC due to the penetration of the low frequency band.

  Two effects lead to better accuracies of the low-frequencies SIC retrievals in regions of high Sea ice concentrations: 1) some of the noise sources have less impact such as sea-ice type, snow depth, snow scattering, among others, and 2) that the TB of sea ice and water are more distant at low frequency bands, resulting in a larger dynamic range for sea-ice concentration retrievals as discussed in Lavergne et al., 2018**.**

7.- Correlation analysis between SIC and Tsnow-ice from IMBB data

The objective of this section is to assess the correlation between the SIC algorithms and the temperature in the snow-ice interface. A priori, we expect that the low frequency bands present higher correlation to temperature.

The report from Lise Kilic with title 'Improving the effective temperature estimation over sea ice using low frequency microwave radiometer data and Arctic buoys' studies which are the TB bands from AMRS2/E that are more sensitive to the snow-ice interface temperature. She concluded that TBs at 10GHz and 6GHz bands are the most sensitive ones, and also that the V-pol is more sensitive than the H-pol.

For doing the above mentioned analysis we have used the files called SICCI-RRDP-ASCAT-vs-AMSR2-vs-ERA-vs-IMBCRREL20XX.text which contains AMSR2 data, collocated with IMBB profilers data. Moreover, we use only those pixels with SIC from SICCI2 algorithms, larger than 80% SIC. We have done the analysis with AMSR2 data, for years 2012 (5 buoys), 2013 (2 buoys) and 2014 (1 buoy) and only data from November to April is considered.

To determine the temperature of the snow-ice interface, we have analysed the temperature profile to find the kink which shows the interface (figures not shown). Finally, the data from the sixth sensor (called T(4)) of IMBB profilers is used as the Temperature between snow-ice mediums. The matlab program from Lise Kilic, attached in her report, has also been used to determine the value of Tsnow-ice. This program looks for the change on the slope of the temperature profile, and considers the depth of the snow-ice interface when the maximum positive derivative slope is present. However, we have found a lot of variability on that depth using this program. So we preferred to keep the sixth sensor data.

The correlation between SIC and Tsnow-ice for data from different buoys for years 2012 to 2014 is computed and is shown in figure 5. Left is the correlation results considering Tsi as the temperature at thermistor number 6 and right, is considering Tsi as the temp. at thermistor number 9. Bottom figure shows the correlation with different thermistors depth, which has been selected using Kilic matlab code. Very different results are obtained within the three cases, and even different correlation signs: the first two correlations are positive and negative, while with Kilic method correlations are always negative (we cannot explain why). All correlations are lower than 0.5 in all cases, so it means that the Tsi has little impact on the SIC maps.

Being aware the considering Tsi as the temperature of a fix thermistor is a rough approximation, (since this depth might change with time and positions) we prefer to continue the analysis with the fixed thermistor at the 6^{th} depth.

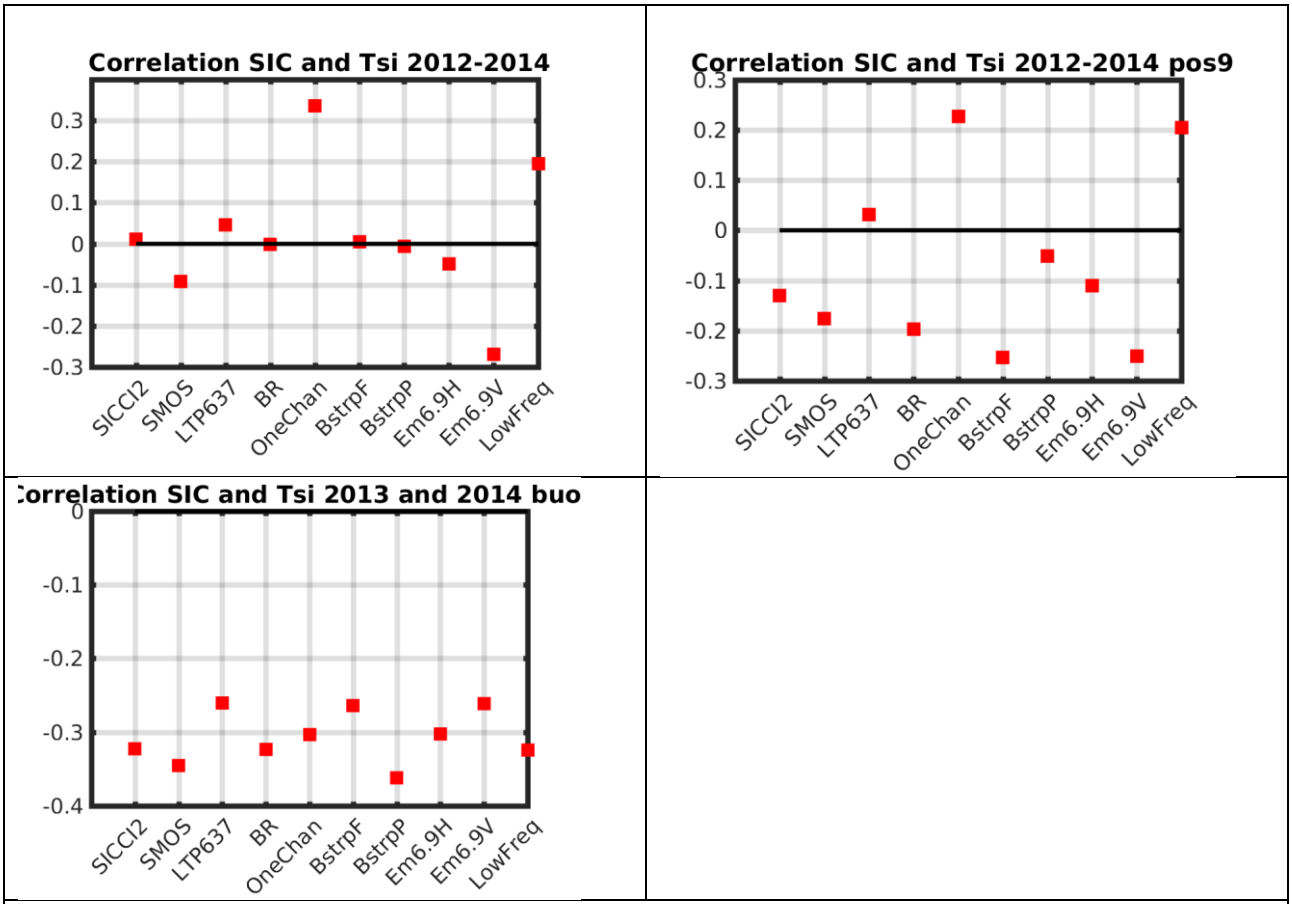

Figure 4: Correlation for all the buoys for years 2012-2014. Top-Left: Tsi computed as T at depth position 6. Top-Right: Tsi computed as T at depth position 9. Bottom: with Tsi computed with the Kilic program (Kilic, 2017).

Year 2014, even choosing only winter period (Nov- April), several measurements show very low SIC and the variability of Tsi is larger.

Using all 3 years of data and considering the fixed thermistor at position 6th (top-left figure), the SIC algorithms, which present higher correlation to Tice-snow are the OneChannel, Emis6.9V and LowFreq models, even though the correlations are not relevant. The high correlation with the Em6.9V SIC is expected since this method uses the value of Tist from NWP to compute the SIC. It is interesting to observe that in some algorithms the correlation is negative.

Conclusion: We can state that the correlations between SIC and Tice-snow is very variable depending on the year, and the depth of the thermistors of the buoys. In general, the SIC algorithms, which present higher correlation to Tice-snow (considering it the 6th thermistor) are the Emis6.9V, OneChannel, and LowFreq models. However, the correlations are quite low. **These algorithms, which show higher correlation use the low frequency bands and vertical polarization.** This is completely in line with the results from Lise Kilic (Kilic, 2017), which states that the largest correlation between TB and Tsi is observed in the low frequencies bands and with the vertical polarization.

On the contrary, these models are the ones that present less STD in the first part of the study, showing a compromise between them. **One could infer that the SICCI 2 model is the most stable, with low STD variability and presents low correlation with temperature.**

The scatterplots and the slope between SIC and Tsi (considered as the 6th thermistor) are plotted in Figure 5, which are an indication of the relation between them. Again, the algorithms, which present larger slope is One Channel, Two Channel and LowFreq algorithms. This confirms that the algorithms using Low frequency bands are more sensitive to temperature of ice. Authors do not see any relation between the methodology used to retrieve SIC (frequency or polarization ratio) and the Tsi value.
We should also take into account that in this section we are comparing measurements from one point (buoy) with the satellite footprint of 25Km resolution. This mismatch produces representation errors. Small scale variability near the buoy will not be observed by the satellite measurements, while might be observed by the buoy sensor. Therefore, this comparison results might introduce errors. Another analysis to determine the sensitivity of SIC to snow-ice temperature would be to compare the satellite footprint with a NWP modelled temperature at similar resolution.

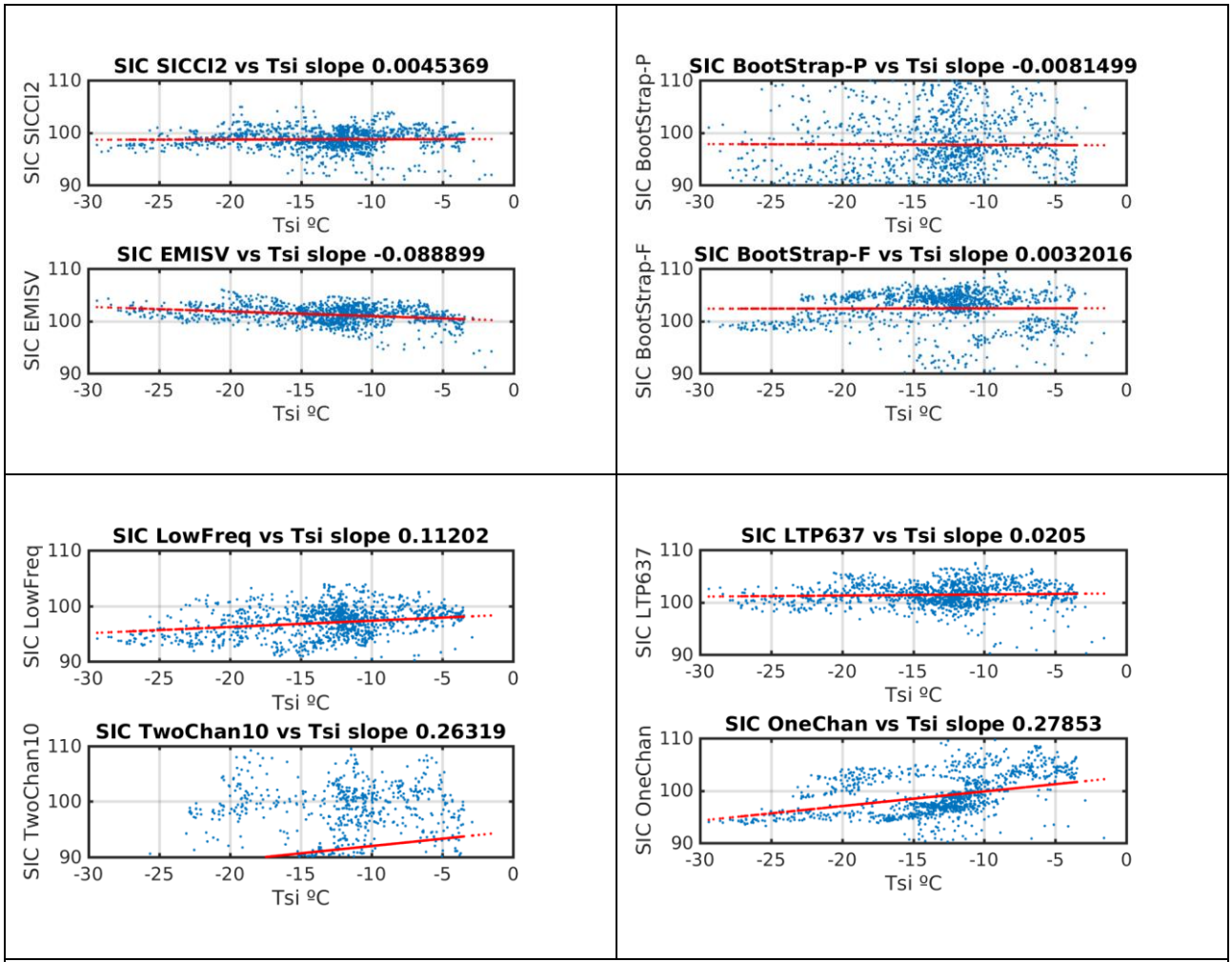

Figure 5: Scatterplot and slope of SIC vs Temperature of snow-ice interface, using Tsi from thermistor number 6.

8.- Correlation analysis between SIC and snow depth using OIB data

With the objective to analyze the reason for the abrupt changes on the systematic bias maps (section 6) near Ellesmere Islands, we use Operation Ice Bridge (OIB) data collocated with AMSR from the RRDP database. We would like to see if bias on SIC could be caused by the snow depth dependence, thin ice, etc. Figure 6 shows the snow depth and ice climatology for the Arctic Region.

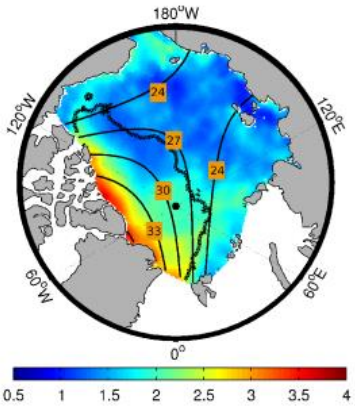

Fig. 1. Arctic sea ice properties and the Arctic sea ice area as defined in this study. Annual mean sea ice thickness from ICESat is shown in colour (m). The line of 50 % multi-year ice fraction is plotted as a thick contour line. Both parameters are given as the average during the 2005–2007 ICESat campaigns. Climatological winter (October–April) snow depth from Warren (1999) from 1954 to 1991 is given as the labelled thin contour lines in centimetres.

Figure 6: Snow annual sea ice thickness and climatological winter snow depth, from Zygmuntowska et al. (2014).

The report from Lise Kilic with title 'Improving the effective temperature estimation over sea ice using low frequency microwave radiometer data and Arctic buoys' studies the TB bands from AMRS2/E which are more sensitive to the snow depth using the OIB data from 2013. The report conclude that the best channels found to retrieve the snow depth variability are the 6.9 GHz V-pol, 18 GHz V-pol and 36.5 GHz V-pol. So following this conclusion we should expect that the algorithms that present more dependence on the snow depth (since they use the previously cited bands) would be: Bootstrap F (uses 19/37Ghz V-pol only), Bristol and One channel and LTP637.

The OIB files called SICCI-RRDP-ASCAT-vs-AMSR2-vs-ERA-vs-NERSC-OIB-201403XX.text from the 13,21,26,28 and 31 March 2014 are used.

Only AMSR2 data in the region with longitude between 0º and 130º W have been used to focus the analysis (see Figure 7). Several SIC maps have been computed using described algorithms. Figure 8 shows that certain correlation is observed between the SIC and increase/decrease of snow depth, even though the correlation value varies a lot depending on the SIC algorithms used. In figure 8 the correlation factor and the slope of the regression line is specified for each algorithm used.

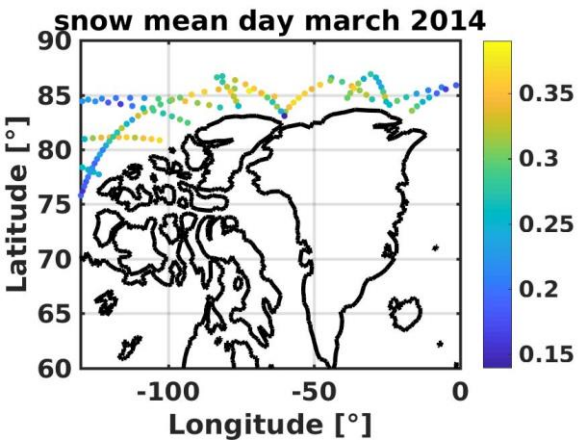

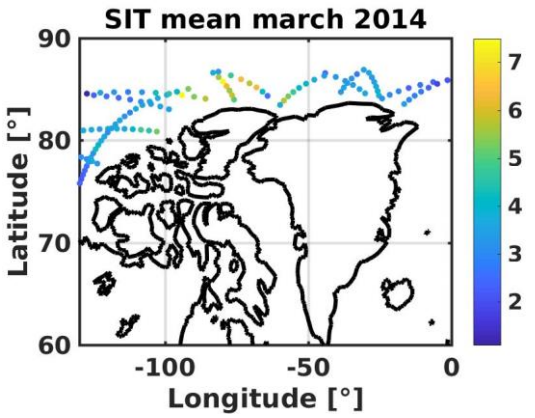

Figure 7: tracks from OIB which has been used for this analysis. The color indicates the mean snow value (in m) in the region.

The OIB measurements are continuous with airplane flight. Then, to perform the collocation, the sensor measurements are averaged into the satellite footprint. Furthermore, the representation error is lower than when comparing satellite footprint with the buoys measurements.

Figure 9 shows the correlation between SIC and the Sea ice thickness (SIT) obtained also from IOB data. Correlations are low, showing a maximum of -0.39 (when using bootstrap F algorithm). Figure 10 computes the correlation between SIC and Skin temperature of the ice, obtained also from the OIB dataset.

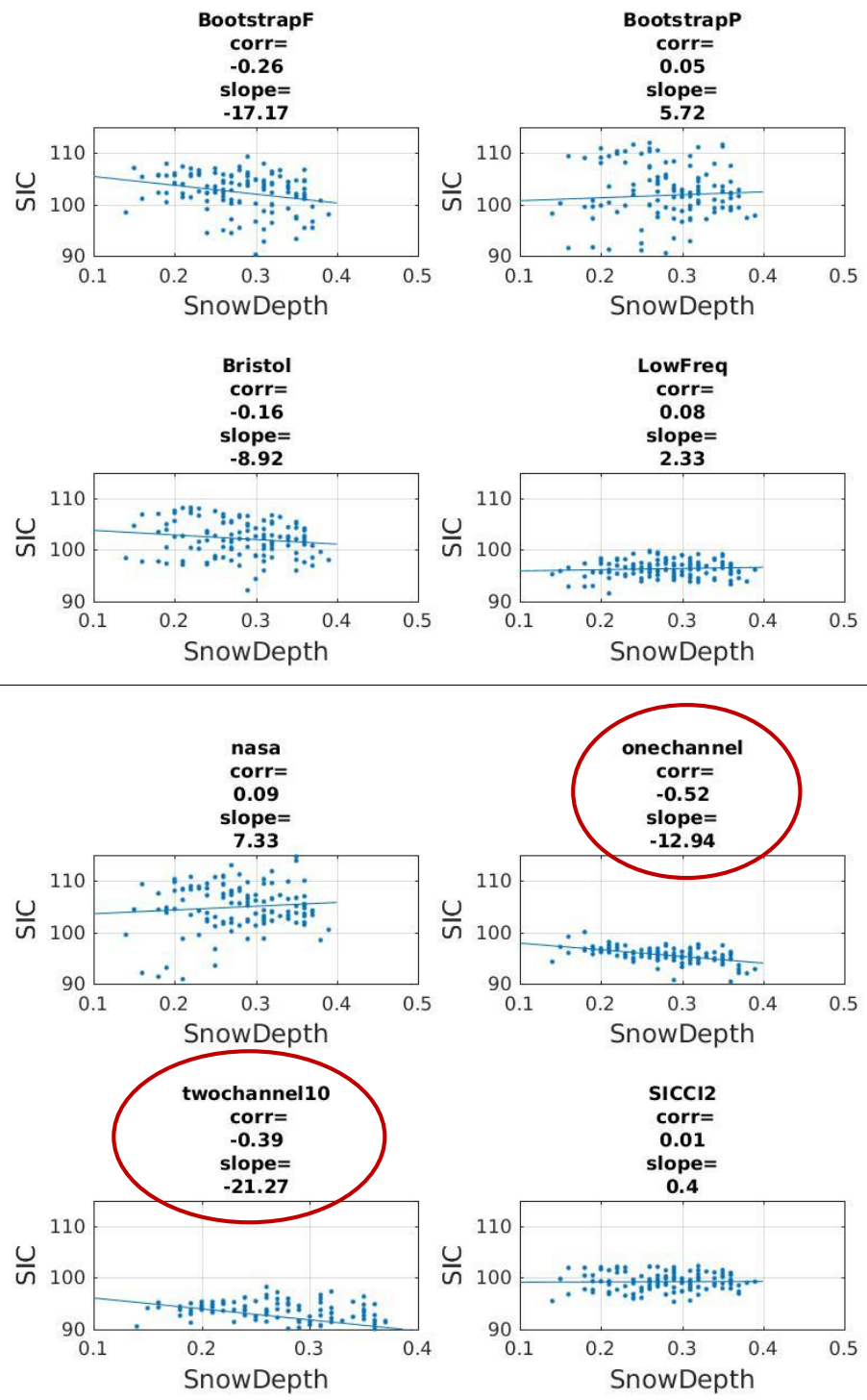

Figure 8: Correlation between SIC and Snow Depth (in m) from OIB

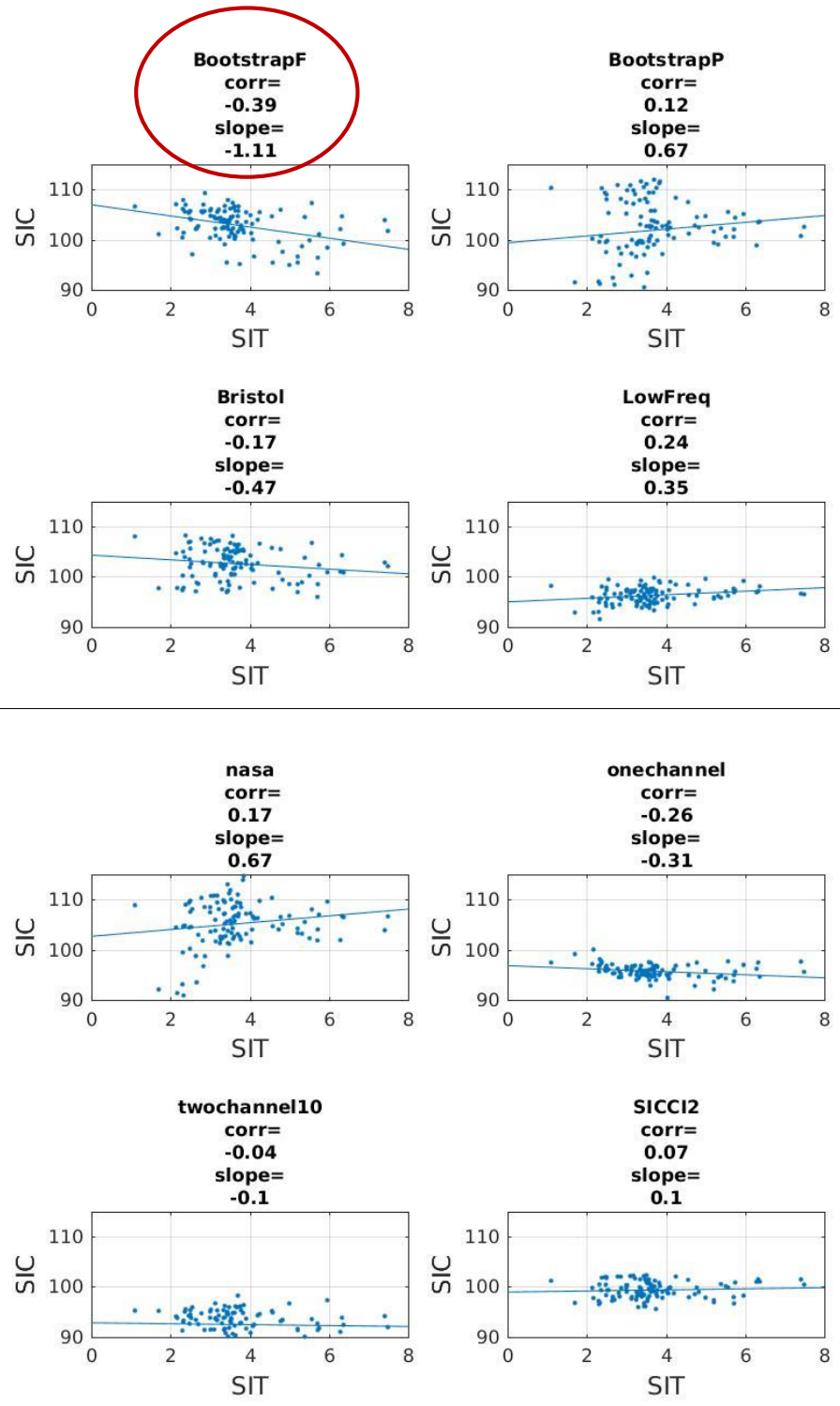

Figure 9: Correlation between SIC and sea ice thickness (in m) from OIB

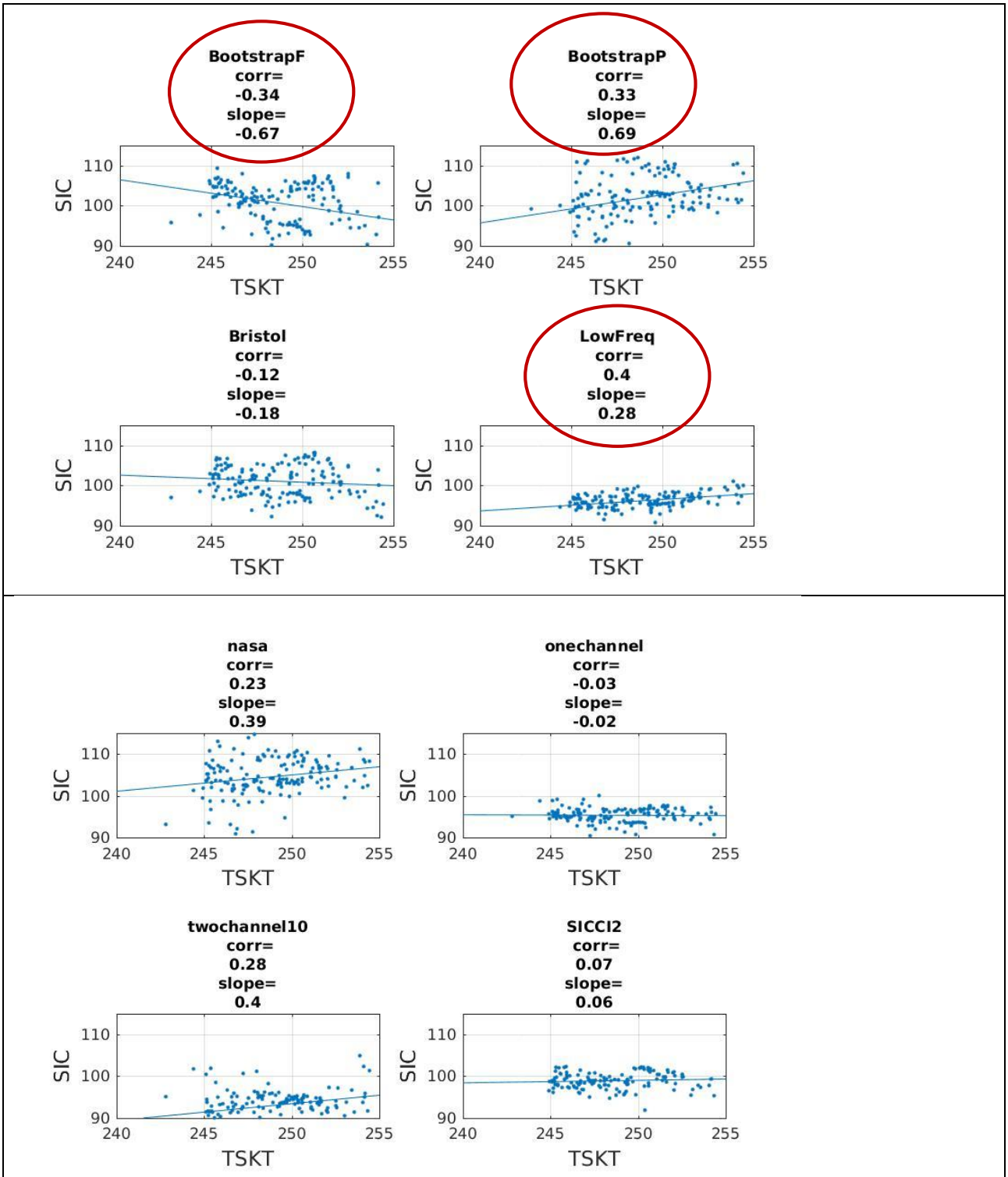

Figure 10: Correlation between SIC and Skin Temperature (in K) from OIB

Conclusions of comparison between SIC and OIB:

Correlations with snow depth:

- Bootstrap F (and Bristol to a lesser extend) shows a light negative correlation with snow depth. This is coherent with figure 6 (bias maps) in the region of Ellesmere Island, where high snow depth is measured with Ice Bridge campaign.
- One Channel and two channels show a significant (but low) correlation to snow depth, with

negative slope, which translates as: high snow lowers the SIC, which might explain the negative bias observed north of Canada in the maps.
- Nasa Team and Bootstrap P show a very light positive correlation with positive slope with snow depth, which could explain the positive bias pattern observed in these systematic maps.
- SICCI2 behaves as insensitive to snow depth.

Correlations with SIT:
- Bootstrap F and Bristol show a negative correlation and slope with SIT which is opposite to what we observe in the maps.
- We do not observe correlation between OneChan and TwoChan and SIT:

Correlations with Tskin parameters:
- Nasa and Bootstrat P have some positive trends with increasing Tskin and show a positive correlation.
- Bootstrap P have similar trend with Tskin, while this is negative for Bootstrap F.

8.- Conclusions

- **SICCI2 and LowFreq algorithms show low systematic and random error and are robust to other geophysical parameters changes** (low sensitivity to snow depth and SIT).

- The algorithms using low frequency bands show lower random noise, which is coherent with other studies.

- These results underline the **potential that future missions like CIMR (Copernicus Imaging Microwave Radiometer)** could have on generating high quality sea ice concentration products.

- The algorithms using the frequency ratio and middle frequency bands (19 and 37GHz), like Bootstrap F and Bristol show a large bias in the regions of multi-year ice.

- SMOS SIC show important errors in some regions of the Arctic. It also shows systematic errors near the hole circle due to acquisition method. Moreover, the low frequency bands, SMOS and OneChannel (1.4Ghz and 6Ghz) are sensitive to thin ice, so presenting errors in region of thin ice like the MIZ zones.

- OneChan shows low systematic error average but results show dependence on snow depth.

- **SICCI2 is the algorithm showing better performances.** However, one should take into account that this model is the only one with dynamic tie points.

- We recommend to explore the possibility to use the 6.9 GHz emissivity values to retrieve SIC due to its low random error performance.

9.- Bibliography

Comiso, J. C.: Characteristics of arctic winter sea ice from satellite multispectral microwave observations, J. Geophys. Res., 91, 975–994, 1986.

Gabarro, C. and Pedersen, L.T. : Intercomparison of OSI-SAF and SMOS-derived sea ice concentration during growing periods: impact of this ice thinckness sensitivity on product quality. OSI SAF Visiting Scientist report, 2016, OSI_AVS_15_03.

Gabarro, C. and Tonboe, R. : The dynamical estimation of summer sea ice tie-points using low frequency passive microwave channels. OSI SAF Visiting Scientist report, 2016, OSI_AVS_16_03.

Gabarro, C, Turiel, A., Elosegui, P., Pla-Resina1, J. and Portabella. 'New methodology to estimate Arctic sea ice concentration from SMOS combining brightness temperature differences in a maximum-likelihood estimator', The Cryosphere, 11, 1987–2002, 2017, https://doi.org/10.5194/tc-11-1987-2017

Ivanova, N., Pedersen, L. T., Tonboe, R. T., Kern, S., Heygster, G., Lavergne, T., Sørensen, A., Saldo, R., Dybkjær, G., Brucker, L., and Shokr, M.: Inter-comparison and evaluation of sea ice algorithms: towards further identification of challenges and optimal approach using passive microwave observations, The Cryosphere, 9, 1797–1817, https://doi.org/10.5194/tc9-1797-2015, 2015.

Kilic, L. 2017, 'Improving the effective temperature estimation over sea ice using low frequency microwave radiometer data and Arctic buoys'. VS-OSISAF Report.

Kern, S., Rösel, A., Pedersen, L. T., Ivanova, N., Saldo, R., and Tonboe, R. T.: The impact of melt ponds on summertime microwave brightness temperatures and sea ice concentrations, The Cryosphere, 10, 2217-2239, 2016. https://doi.org/10.5194/tc-10-2217-2016.

Lavergne, T., Sørensen, A. M., Kern, S., Tonboe, R., Notz, D., Aaboe, S., Bell, L., Dybkjær, G., Eastwood, S., Gabarro, C., Heygster, G., Killie, M. A., Kreiner, M. B., Lavelle, J., Saldo, R., Sandven, S., Pedersen, L. T.'Version 2 of the EUMETSAT OSI SAF and ESA CCI Sea Ice Concentration Climate Data Records', The Cryosphere Discussions, 2018, 10.5194/tc-2018-127.

Markus and D. J. Cavalieri. Snow Depth Distribution Over Sea Ice in the Southern Ocean from Satellite Passive Microwave Data in Antarctic Sea Ice: Physical Processes, Interactions and Variability (ed M. O. Jeffries). pages 19–39. American Geophysical Union, Washington, D. C, mar 1998. ISBN 9781118668245. doi: 10.1029/AR074p0019

Markus, T. and Cavalieri, D. J.: An enhancement of the NASA Team sea ice algorithm, IEEE T. Geosci. Remote, 38, 1387– 1398, 2000

Pedersen, L. T.: Merging microwave radiometer data and meteorological data for improved sea ice concentrations, EARSeL Adv. Remote Sens., 3, 81–89, 1994.

Smith, D. M.: Extraction of winter total sea-ice concentration in the Greenland and Barents Seas from SSM/I data, Int. J. Remote Sens., 17, 2625–2646, 1996.

Tonboe, R. T., Eastwood, S., Lavergne, T., Sørensen, A. M., Rathmann, N., Dybkjær, G., Toudal Pedersen, L., Høyer, J. L., and Kern, S. 2016: The EUMETSAT sea ice climate record, The Cryosphere, 10, 2275-2290, 2016, https://doi.org/10.5194/tc-10-2275-2016

M. Zygmuntowska, P. Rampal , N. Ivanova , and L. H. Smedsrud, 2014, 'Uncertainties in Arctic sea ice thickness and volume: new estimates and implications for trends'. The Cryosphere, 8, 705–720, 2014 www.the-cryosphere.net/8/705/2014/ doi:10.5194/tc-8-705-2014.

ANNEX 1:

The histograms of the SIC spatial bias (computed as described in section 4) during the month from November 2013 to March 2014 have been plot using the AMSR-2 data. Take into that only pixels with SIC larger than 80% are considered to create the histograms (since the analysis is focus only over high SIC regions).

Figures show bi-model histograms for the PR algorithms, with a maximum near 0 (so SIC=1) and another in SIC=1.18 approx. This is because they are sensitive to different ice types and snow types. The algorithms which show less noise, smaller STD, are SICCI2, SMOS and the Frequency rate algorithms (BootstrapF and Bristol), which is coherent with results already analysed.

The SICCI2 algorithm histogram show an abrupt cut just after 1, as previously observed. Lowfreq and OneChan show a large positive tail, but with very few points on those values.

SMOS show a tight distribution having a small STD.

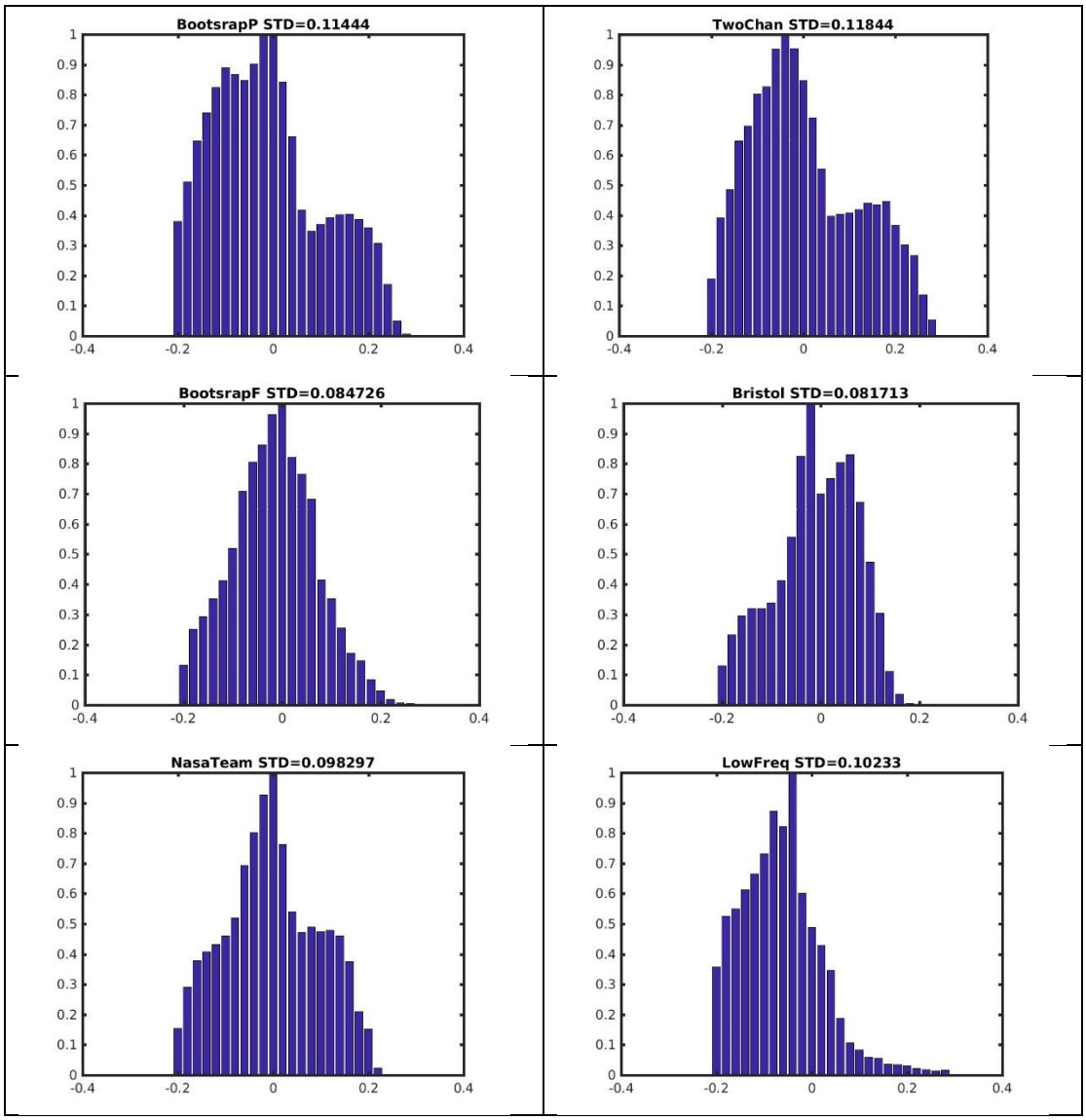

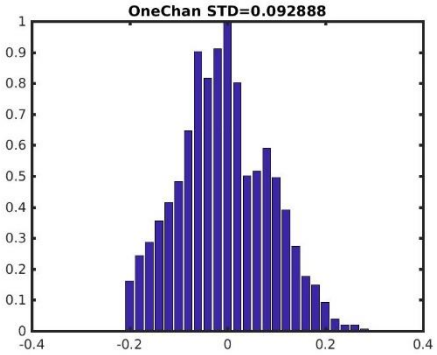

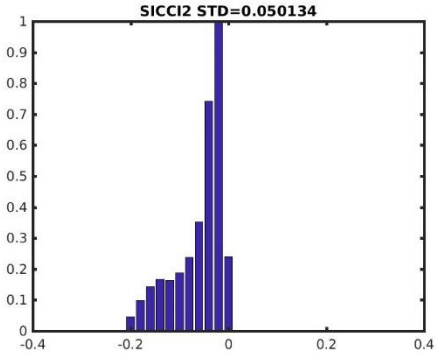

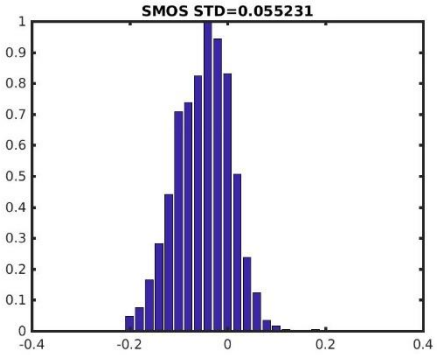

Figure annex : histograms of the averaged SIC -1 during winter time.